Title
Formation of Vibrationally Excited Methyl Radicals Following State-Specific Excitation of Methylamine

Journal
The Journal of Physical Chemistry A, 118(42)

ISSN
1089-5639

Authors
Thomas, James O
Lower, Katherine E
Murray, Craig

Publication Date
2014-10-23

DOI
10.1021/jp508562w

Peer reviewed

Formation of Vibrationally Excited Methyl Radicals Following State-Specific Excitation of Methylamine

James O. Thomas[a], Katherine E. Lower[a], and Craig Murray[b]

Department of Chemistry, University of California, Irvine, Irvine, CA 92697, USA

[a] School of Chemistry, University of Bristol, Bristol BS8 1TS, UK
[b] Email: craig.murray@uci.edu;Telephone: +1 949 824 4218

Abstract

The photochemistry of methylamine has been investigated following state-specific excitation of the S_1 state. 2+1 resonance-enhanced multiphoton ionization was used to detect nascent methyl radical products via the $3p^2A_2''$–$\tilde{X}^2A_2''$ electronic transition. Methyl radicals were formed at all photolysis wavelengths used over the range 222 – 240 nm. The nascent products showed significant rotational excitation and several quanta of vibrational excitation in ν_3, the degenerate C–H stretch. The partially deuterated methyl-d_3-amine isotopologue yielded methyl-d_3 fragments with vibrational distributions entirely consistent with those measured for the fully protiated species; no mixed isotopologues were detected. Energetic constraints require that the vibrationally excited methyl radicals be produced in conjunction with electronic ground state NH_2 $\tilde{X}^2B_1$ radicals on the S_0 surface, negating the previous interpretation that dissociation occurs on the upper adiabat. New *ab initio* calculations characterizing the C–N bond cleavage coordinate confirm the presence of a barrier to dissociation on S_1 that is insurmountable at the photolysis wavelengths used in this work. We propose a "semi-direct" mechanism in which frustrated aminyl H-atom loss on the upper adiabatic potential energy surface leads to internal conversion at the exit-channel conical intersection at extended N–H distance on its return. It is proposed that C–N bond cleavage then occurs promptly and non-statistically on the S_0 surface.

Keywords: photochemistry, methylamine, photodissociation dynamics, methyl radicals

Introduction

The photochemistry of methylamine after excitation in its first UV absorption band has been the subject of significant experimental[1–17] and theoretical[18–24] attention. Methylamine is the simplest alkyl-substituted analog of ammonia, which provides an almost textbook example of the influence of exit-channel conical intersections on photodissociation dynamics.[25–30] The absorption spectra and the electronic states of ammonia and methylamine share several important characteristics and lead to the expectation of similar behavior. The photochemistry of methylamine, however, is far richer than that of ammonia; five dissociation pathways have been experimentally identified after excitation in the structured long-wavelength absorption band:

$CH_3NH_2 \rightarrow H + CH_3NH$ $\Delta H = 4.451$ eV (R1)

$\rightarrow H + CH_2NH_2$ $\Delta H = 3.794$ eV (R2)

$\rightarrow H_2 + CH_2NH$ $\Delta H = 1.314$ eV (R3)

$\rightarrow CH_3 + NH_2$ $\Delta H = 3.633$ eV (R4)

$\rightarrow CH_4 + NH$ $\Delta H = 3.170$ eV (R5)

The thermochemical data shown above are for electronic ground state products and have been derived from standard enthalpies of formation at 298 K tabulated in the NASA-JPL evaluation.[31]

The first UV band of methylamine spans the 190–240 nm wavelength range and displays diffuse vibronic structure. In the Franck-Condon region, the first electronically excited

state $\tilde{A}^1A'$ (henceforth labelled S_1 for convenience) is of bound *n*,3s Rydberg character but rapidly evolves into a dissociative *n*,σ* state upon extension of either the C–N or an N–H bond.[32,33] Excitation to S_1 is accompanied by a geometry change about the N-atom from pyramidal to effectively planar. The vibronic structure in the spectrum has been assigned to progressions in the aminyl wagging mode, ν_9 and a second mode that has been ascribed variously to either the methyl rock, ν_7, or the C–N stretch, ν_8.[32–34] The most detailed spectroscopic analysis comes from Kim and co-workers, who have recorded 1+1 REMPI spectra of methylamine (as well as partially and fully deuterated isotopologues) and modeled the vibronic features using a hindered internal rotor Hamiltonian.[35–37] Spectra of the protiated methylamine show homogeneous broadening consistent with a lifetime of 0.38 ps at the origin and decreasing as the excitation energy increases. Analogous spectra of the partially deuterated methylamine-d_2 species display sharper lines, and a longer excited state lifetime of around 8.8 ps. The short lifetime and isotope effect is indicative of predissociation by H-atom tunneling through an exit channel barrier.

Ab initio calculations confirm the presence of a small barrier on the S_1 potential energy surface along the N–H bond dissociation coordinate and a larger one along the C–N dissociation coordinate.[18,19] Considering first extension of the C–N bond in pyramidal geometries, the S_0 state ($\tilde{X}^1A'$) of the parent molecule correlates adiabatically with ground state CH_3 $\tilde{X}^2A_2''$ + NH_2 $\tilde{X}^2B_1$ products, while the S_1 state ($\tilde{A}^1A'$) correlates with electronically excited NH_2 $\tilde{A}^2A_1$. These correlations are reversed in planar geometries resulting in a same-symmetry conical intersection in the exit channel, analogous to that found for NH_3. Representative cuts through the potential energy surfaces and the correlations are shown in Figure 1. Dunn and Morokuma also discuss their one-dimensional cuts through the

potential energy surfaces in terms of a 'ciscoid' geometry, which can be derived from the planar S_1 minimum by a ~90° rotation about the C–N bond. In ciscoid geometries, the S_1 state has $^1A''$ symmetry and the adiabatic correlations follow those of planar geometries. A very similar picture arises upon extension of an N–H bond, which is also illustrated in Figure 1; ground state parent correlates with ground state H + CH_3NH $\tilde{X}^2A''$ products, and excited state with excited state CH_3NH $\tilde{A}^2A'$ in pyramidal geometries. These correlations again reverse in planar or ciscoid geometries, giving rise to a conical intersection in the exit channel. This conical intersection has been the subject of particular theoretical interest recently, and as we argue below, provides an important means of internal conversion, transferring population from S_1 to S_0.[20,21,23] For convenience in the following, we indicate all electronically excited products with an asterisk.

End-product analysis following broadband excitation of methylamine across the first absorption band allowed Michael and Noyes to identify four active dissociation pathways, identified above as R1–R4.[4] The major pathway is loss of an H-atom, for which the quantum yield was estimated to be $\Phi = 0.75$. The bulk of H-atom production comes from the aminyl group (R1) with a small contribution from the methyl group (R2). Direct production of molecular hydrogen (R3) was identified as a minor pathway ($\Phi = 0.10$) while the C–N bond cleavage pathway (R4) to produce CH_3 and NH_2 radicals was thought to account for $\Phi < 0.05$. Recently, we have conclusively identified a fifth dissociation pathway (R5) that results in the formation of methane and NH $X^3\Sigma^-$ radicals.[17] The branching fraction for R5 has not been determined, but is likely to be small.

The bulk of experimental studies to date have focused on the dominant H-atom loss channel. Ashfold and co-workers used hydrogen Rydberg-atom photofragment translational spectroscopy (HRA-PTS) to investigate the photodissocation of methylamine and deuterated isotopologues over a range of wavelengths spanning the first absorption band.[6,7] The total kinetic energy release spectra were bimodal, suggesting that at least two mechanisms lead to the formation of H (or D) atoms, in agreement with earlier PTS experiments performed by Waschewsky *et al*.[5] The fast component was argued to be consistent with prompt dissociation via the exit channel conical intersection leading directly to H + CH_3NH. The slow component was indicative of statistical dissociation on S_0, albeit still leading to scission of the strong N–H bond, suggesting that internal conversion occurs at extended N–H bond lengths. More recently, Ahn *et al.* have also exploited the vibronic structure to state-selectively dissociate CH_3NH_2 (CH_3ND_2) via the 0_0^0, 9_0^1, 9_0^2 (and 9_0^3) bands, measuring H or D-atom kinetic energy distributions using velocity map ion imaging (VMI).[10] While VMI generally has lower resolution than the HRA-PTS technique, similar bimodal kinetic energy distributions were observed. Bar and co-workers have performed numerous vibrationally-mediated photodissociation studies, demonstrating mode-specific dissociation dynamics,[8,9,11–15] while electronic action spectroscopy studies of CD_3NH_2 photodissociation showed that increasing the photon energy led to increasing yields of both H and D atom fragments.

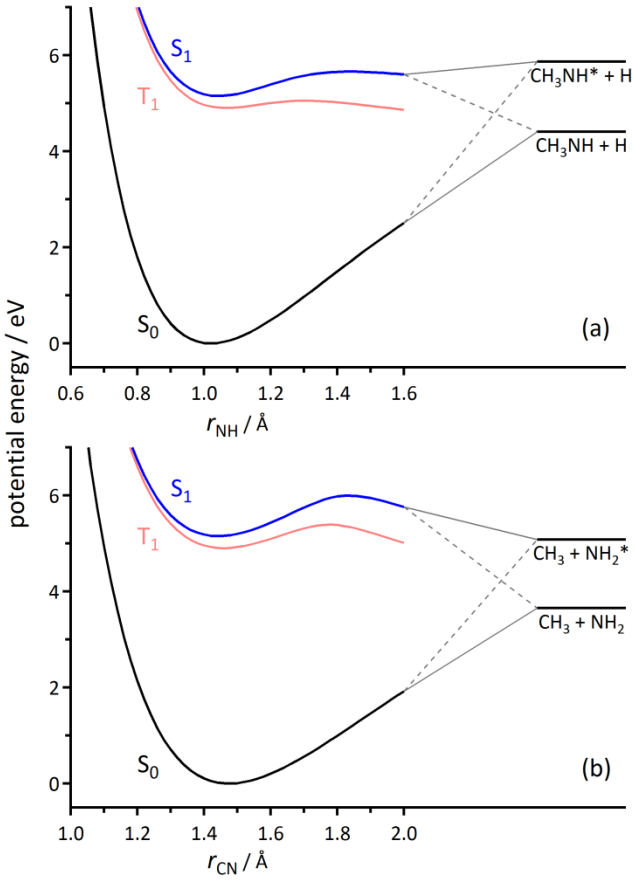

Figure 1. Schematic one dimensional potential energy curves along the (a) N–H and (b) C–N cleavage coordinates for the S_0, S_1 and T_1 states of methylamine calculated at the (EOM-)CCSD/aVDZ level. All other geometrical parameters were held fixed at those of the appropriate minimum. Zero-point energies are not included. At longer range, adiabatic correlations in pyramidal geometries are represented by solid lines and in planar (or ciscoid) geometries by dashed lines.

Waschewsky *et al.*[5] explicitly identified the pathway R4 in their PTS experiments by momentum matching ND_2 and CH_3 fragments following photodissociation of CH_3ND_2 at 222 nm and to date, this is the only collision-free study of this pathway reported in the literature. Excitation at 222 nm provides 5.58 eV of total energy, which is slightly greater than the contemporary calculated barrier on S_1 of 0.47 eV.[19] The translational energy

distribution peaked away from zero, indicative of direct dissociation on a repulsive potential, and did not extend beyond 17.5 kcal mol^{-1} (~0.76 eV), consistent with dissociation exclusively leading to electronically excited ND_2* products. The mechanism proposed involved direct dissociation on S_1 by passage over the barrier, avoiding the exit channel conical intersection, and leading to CH_3 and electronically excited NH_2* radicals.

In this paper, we examine the C–N cleavage pathway by directly detecting the nascent methyl radical photofragments. Methylamine and methyl-d_3-amine were state-selectively excited at several wavelengths that correspond to previously characterized vibronic transitions in the first absorption band providing total energy ranging from 5.17–5.58 eV. 2+1 REMPI spectra of nascent methyl and methyl-d_3 radical products show a significant fraction of the available energy is partitioned into vibrational excitation. Complementary *ab initio* calculations characterize important stationary points on the potential energy surfaces. The new results are incompatible with the mechanism of direct dissociation on the upper surface to produce CH_3 and NH_2* fragments that was suggested in earlier work. We propose an alternative indirect, but non-statistical, mechanism that involves frustrated N–H bond cleavage followed by internal conversion and dissociation on the S_0 surface.

Experiment

Nascent products of methylamine photodissociation were detected by REMPI in a Wiley-McLaren time-of-flight mass spectrometer (TOF-MS). Methylamine and methyl-d_3-amine (Aldrich, 10% in Ar, 99.5% D) were expanded into the source chamber of the TOF-MS using a solenoid pulsed valve (General Valves, Series 9) and a stagnation pressure of ≤ 1 bar. Some preliminary experiments were also performed using trimethylamine (Aldrich, 1% in

Ar). The resulting free-jet expansion passed through a skimmer (Beam Dynamics, 1 mm diameter) to produce a molecular beam which traveled into the ionization chamber between repeller and extractor electrodes. The electrode assembly, which also included an Einzel lens, accelerated and focused ions onto a microchannel plate (MCP, Photonis) detector positioned at the end of a 1.2 m long field-free drift tube. The source chamber of the spectrometer was evacuated with a water-baffled diffusion pump (Leybold DIP 3000 S), while the ionization and drift tubes were evacuated using turbomolecular pumps (Leybold Turbovac 1100 C and 361). The typical base pressure in the source chamber was 2×10^{-7} mbar and this increased to approximately 6×10^{-5} mbar during valve operation. The pressure in the ionization and drift regions of the apparatus increased only slightly during valve operation from typical base pressures of around 2×10^{-8} mbar.

The molecular beam was intersected perpendicularly around 15 cm from the skimmer in the centre of the ionization chamber by spatially overlapped, counter-propagating photolysis and probe laser beams. The UV photolysis beam was generated by frequency doubling the fundamental output of a Nd:YAG-pumped dye laser (Spectra Physics PDL-3, Continuum Surelite II–10) operating with coumarin dyes between 440 – 480 nm in a β-barium borate (BBO) crystal. The pulse energy was intentionally kept low (typically < 300 μJ per pulse) and directed into the vacuum chamber unfocused to minimize potential contributions from multiphoton processes. An f = 500 mm lens was introduced when recording 1+1 REMPI spectra of the parent amines. UV probe laser radiation was generated using a second Nd:YAG-pumped dye laser system (Labmda Physik ScanMate 2, Continuum Surelite II–10) operating between 655 – 690 nm using oxazine dyes. The fundamental output of the probe dye laser was also frequency doubled in a BBO crystal and

focused into the interaction region of the TOF-MS using an f = 300 mm lens. UV probe pulse energies were typically around 1.0 – 1.5 mJ. Wavelength calibration was performed in the visible using a Ne optogalvanic lamp integrated into the probe dye laser, and further checked using a wavemeter (Coherent Wavemaster).

Synchronization of the pulsed valve and lasers was achieved using two digital delay generators (SRS DG535 and Quantum Composers 9514+). The MCP signal output was coupled to a digital storage oscilloscope (LeCroy). Custom data acquisition software was written in LabVIEW (National Instruments) to acquire time-of-flight mass spectra on a shot-by-shot basis. Multiple gates could be integrated while scanning the wavelength of the photolysis or probe laser to generate mass-resolved spectra. Two types of measurement were performed. First, the photolysis laser was fixed on previously characterized vibronic transitions of the parent amines and resonance-enhanced multiphoton ionization (REMPI) spectra of the nascent photodissociation products were recorded. Secondly, photofragment excitation (PHOFEX) spectra were acquired by fixing the probe laser frequency on a specific REMPI transition of a photoproduct while scanning the photolysis laser frequency. Additional 1+1 REMPI spectra of the parent amines were also recorded. Relative photolysis and probe laser pulse energies were monitored during data acquisition by directing reflections from quartz flats onto Si photodiodes.

In addition to the experimental measurements, complementary a*b initio* calculations were carried out to characterize various stationary points (minima and transition states) on the S_0, S_1 and T_1 potential energy surfaces. All calculations were performed using the Molpro 2012.1 package.[38,39]

Results

Trimethylamine vs. methylamine

Preliminary 2+1 REMPI survey spectra of nascent CH_3 radical products were recorded following the photodissociation of trimethylamine and methylamine at ~222 nm. Trimethylamine was initially excited near the peak of the weakly structured first absorption band at 222.0 nm while methylamine was state-selectively excited at 222.2 nm, which corresponds to the $7_0^2 9_0^2$ band, as assigned by Park *et al.*[37] Low-resolution spectra were recorded by integrating the m/z = 15 ion signal as a function of probe laser wavelength over the approximate range 329 – 338 nm. This range was selected to cover bands associated with the $3p^2A_2''$–$\tilde{X}^2A_2''$ two-photon transition of the CH_3 radical that have been previously characterized by Hudgens *et al.*[40] A delay of 20 ns between the photolysis and probe laser beams was used for methylamine experiments. The S_1 state of trimethylamine, however, is relatively long lived with a fluorescence lifetime of 8.4 ns and the cation can be generated by absorption of a second photon of either the photolysis or probe laser wavelength, before dissociating to produce CH_3^+ fragments.[41] In trimethylamine experiments, a more dilute gas mixture and a longer time delay between the photolysis and probe lasers (50 ns rather than 20 ns) were used to favor detection of direct photodissociation products over background signals. The longer delay in particular removed contributions to the CH_3^+ ion signal arising from 1+1 and 1+1′ REMPI of the parent molecule.

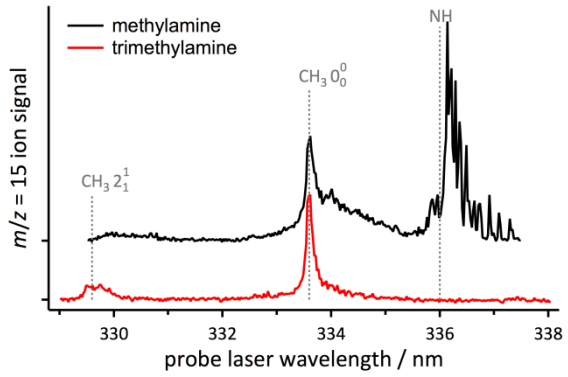

Figure 2. Low-resolution REMPI survey spectra of nascent m/z = 15 products resulting from the photodissociation of trimethylamine (red) and methylamine (black, offset vertically) and at a photolysis wavelength of ~222 nm. Origins of the $3p^2A_2''$–$\tilde{X}^2A_2''$ 2_1^1 and 0_0^0 bands of the CH_3 radical and the $D^3\Pi$–$X^3\Sigma^-$(0,0) band of the NH radical are indicated.

Low-resolution REMPI survey spectra of methylamine and trimethylamine photoproducts with m/z = 15 are shown in Figure 2. All features present in the spectra required that the photolysis beam precede the probe beam in time and the signal intensity decayed over many tens of ns with increasing delay time, which is attributed to fly-out from the relatively small probe volume. After photolysis of trimethylamine, two distinct bands of the 3p–$\tilde{X}$ electronic transition of CH_3 are evident: the Q-branch that dominates the 0_0^0 band at a one-photon wavelength of 333.6 nm and the 2_1^1 band at 329.6 nm. The latter indicates formation of CH_3 radicals with (at least) one quantum of vibrational excitation in ν_2, the out-of-plane (umbrella) bend. The spectrum obtained after photodissociation of methylamine is markedly different. The 2_1^1 band of CH_3 is absent, while the 0_0^0 band is accompanied by a series of vibrational hot bands to longer wavelength. Most striking, however, is the presence of an additional, rotationally structured band at 336.0 nm, which is absent following photodissociation of trimethylamine. As discussed elsewhere,[17] this

feature is assigned to the $D^3\Pi$–$X^3\Sigma^-$(0,0) transition of the NH radical, detected via a 3+1 REMPI process, based on PGOPHER simulations using the band origin and other spectroscopic constants reported in a 2+1 REMPI study at 224 nm by Clement *et al.*[42,43] Energy conservation requires NH $X^3\Sigma^-$ be formed in conjunction with CH_4. This dissociation pathway must involve the triplet surface and the mechanism is postulated to involve a roaming-mediated intersystem crossing (ISC). In this paper, attention is focused on the CH_3 (and CD_3) photofragments resulting from state-selective photodissociation of methylamine and methyl-d_3-amine.

State-selective photodissociation of CH_3NH_2 and CD_3NH_2

The first absorption bands of the parent amines are dominated by progressions in the aminyl wag (ν_9) and methyl rock (ν_7) modes. By tuning λ_{phot}, the parent amines can be selectively excited to different vibronic levels to explore mode-specific photochemistry. Assignments from the 1+1 REMPI study by Park *et al.*[37] were used to identify the 0_0^0, 9_0^1, 7_0^1, 9_0^2 and $7_0^2 9_0^2$ bands of methylamine and the 0_0^0, 9_0^1, 7_0^1, 9_0^2 and $7_0^1 9_0^4$ bands of methyl-d_3-amine, which span 222 – 240 nm. Following state-specific excitation of the parent amine, the probe laser wavelength was scanned over the previously identified bands associated with the 3p–$\tilde{X}$ electronic transition of the nascent CH_3 and CD_3 photoproducts while the m/z=15 (CH_3^+) or m/z = 18 (CD_3^+) ion signal was integrated. Precise photolysis wavelengths within each band (summarized in Table 1) were selected to maximize the intensity of product ion signals in the time-of-flight mass spectrum and consequently they differ slightly from the band origins reported by Park *et al.*[37]

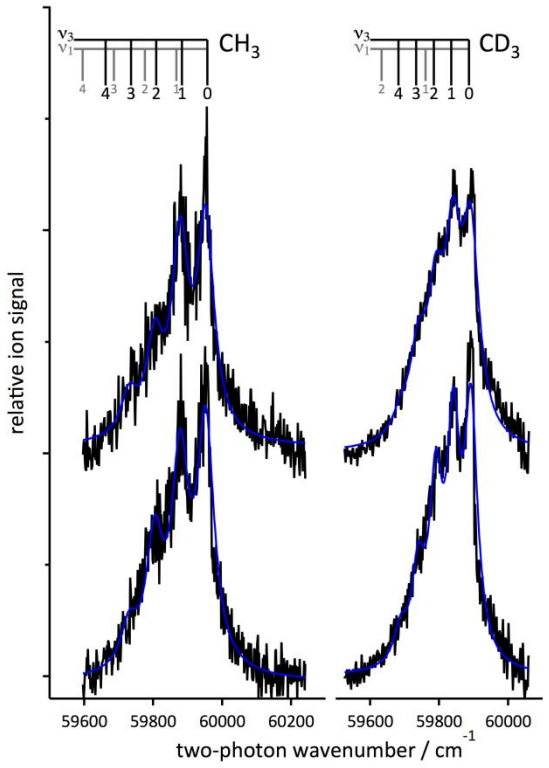

Figure 3. 2+1 REMPI spectra of nascent CH_3 and CD_3 radicals formed following state-selective photodissociation of CH_3NH_2 or CD_3NH_2 via the 0_0^0 (upper) and 9_0^2 (lower) bands. Band origins for the $1_{n''}^{n'}$ and $3_{n''}^{n'}$ sequences of the $3p^2A_2''$–$\tilde{X}^2A_2''$ transition of CH_3 and CD_3 are indicated by ladders. Fits of the experimental spectra to multiple Lorentzian functions are shown in blue.

Figure 3 shows 2+1 REMPI spectra of CH_3 and CD_3 products after excitation of the parent amines to S_1 on the 0_0^0 and 9_0^2 bands. Spectra acquired after excitation of the other bands were almost identical. The CH_3 (CD_3) REMPI signal intensity increased with decreasing photolysis wavelength although this trend was not quantified; for all bands, the signals were small, consistent with this being a relatively minor photodissociation channel.[4,5] The maxima at two-photon wavenumbers of ~59950 cm^{-1} and ~59890 cm^{-1} can be assigned to the 3p–$\tilde{X}$ 0_0^0 bands of CH_3 and CD_3 products, respectively, and are accompanied by series of additional, regularly spaced peaks to lower wavenumber. In the CH_3 spectra, the spacing

between successive peaks is approximately $\Delta\bar{\nu} = -74$ cm^{-1}, while the analogous spacing in the CD_3 spectra is about $\Delta\bar{\nu} = -51$ cm^{-1}.

The regularity in the peak-to-peak separation is attributed to band sequences arising from photolytic production of vibrationally excited radicals. The magnitude of the wavenumber separation in the CH_3 spectra is consistent with the wavenumber shift of the 3_1^1 band from the 0_0^0 band reported in IR/UV double resonance studies[44] and the additional features are assigned to a sequence in the degenerate CH stretch (ν_3, e'), $3_{n''}^{n'}$ where $n' = n'' = 1, 2, 3\ldots$ While a sequence in the symmetric CH stretch (ν_1, a_1') would show similar red-shifts of $\Delta\bar{\nu} = -90$ cm^{-1}, assignment to a sequence in $3_{n''}^{n'}$ shows marginally better agreement (particularly as n increases) and is also more consistent with the CD_3 measurements described below. Excitation in either of the lower frequency modes, the out-of-plane bend (ν_2, a_1'') and the in-plane deformation (ν_4, e'), can be discounted. The 2_1^1 band is significantly blue-shifted relative to the 0_0^0 band ($\Delta\bar{\nu} = +728$ cm^{-1}) due to the large increase in the frequency of this mode upon electronic excitation, and is not observed in the experimental spectra. The ν_4 vibration has not been characterized in the gas phase, but Ar matrix studies and *ab initio* harmonic frequency calculations suggest that the 4_1^1 band should display a wavenumber shift of $\Delta\bar{\nu} = +50$ cm^{-1} relative to the 0_0^0 band.

The wavenumber of ν_3 in the $3p^2A_2''$ state of CD_3 has not been reported previously, but the assignment of a $3_{n''}^{n'}$ sequence can be made by analogy with the CH_3 spectra. Based on previously reported vibrational wavenumbers, the 1_1^1 band is predicted to show a shift of $\Delta\bar{\nu} = -126$ cm^{-1}, which is over twice that observed. The 2_1^1 band of CD_3 was also identified in the 2+1 REMPI spectroscopy work of Hudgens *et al.*[40] and is found at $\Delta\bar{\nu} = +580$ cm^{-1}

relative to the origin band. As with CH_3, ν_4 in the electronic ground state of CD_3 has been observed previously only in matrices and in conjunction with *ab initio* calculations, a probable shift in the 4_1^1 band of only $\Delta\bar{\nu} = -17$ cm^{-1} is anticipated.[45] The assignment of the observed features to the $3_{n''}^{n'}$ sequence implies that ν_3 of CD_3 has a wavenumber of 2330 cm^{-1} in the $3p^2A_2''$ state.

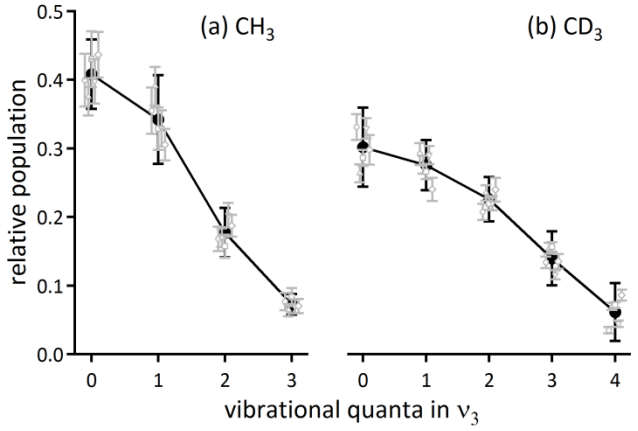

Figure 4. Nascent vibrational population distributions derived from 2+1 REMPI spectra of (a) CH_3 and (b) CD_3 products of methylamine and methyl-d_3-amine photodissociation, respectively. Distributions are shown following initial excitation to various vibronic states in gray and the average in black.

Detailed spectral band simulations are problematic due to the lack of availability of rotational constants, particularly for vibrationally excited levels, but the experimental spectra are insufficiently resolved to justify this approach. The CH_3 and CD_3 spectra were modeled as a sum of multiple Lorentzian functions, chosen to approximate the individual vibronic band contours and provide a semi-quantitative estimate of the vibrational distribution. During the fitting process, the band origins were fixed and the individual Lorentzian functions were constrained to have the same width. The resulting fits are

shown superimposed on the experimental spectra in Figure 3 and the vibrational population distributions derived from this, admittedly rather crude, approach are shown in Figure 4. In this analysis, it has been assumed that the relative REMPI detection sensitivities are the same for all vibronic bands. We note that Zhang *et al.*[46] reported a factor of 3.4 ± 0.6 greater sensitivity for the 3_1^1 band over the 0_0^0 band in IR-UV double resonance experiments. In practice, the ionization rate will be influenced by experimental factors such as the probe laser pulse energy and focusing conditions. The relative detection sensitivities under our experimental conditions have not been characterized although the similarity of the CH bond lengths in the ground and Rydberg states of the neutral CH_3 and the ground state of the CH_3^+ cation (1.076 Å, 1.086 Å and 1.095 Å, respectively) suggests that Franck-Condon factors for both the resonant and ionization steps should be highly diagonal. Consequently, we make no correction for the relative detection sensitivity of the vibrationally excited radicals.

Within the uncertainties of the measurements, the vibrational population distributions are identical, regardless of which vibronic state of the parent molecule was initially excited. The population distributions peak in the vibrationless level and decrease monotonically, although the majority of methyl or methyl-d_3 radical products are formed vibrationally excited: 59 ± 3 % of CH_3 and 70 ± 3% of CD_3 photoproducts are produced with one or more quanta in ν_3. By taking an average over all bands and modeling the ν_3 vibrational energy levels as a harmonic oscillator, the mean energy partitioned into vibration is calculated to be $\langle E_{\mathrm{vib}} \rangle$ = 0.356 ± 0.059 eV for CH_3 and 0.402 ± 0.044 eV for CD_3. These fractions correspond to 18–25% of the total available energy and are summarized in Table 1.

Finally, the m/z =15 (CH_3^+), m/z = 16 (CH_2D^+) and m/z = 17 (CHD_2^+) mass channels were also integrated while recording 2+1 REMPI spectra of CD_3 photoproducts during experiments with methyl-d_3-amine. The 0_0^0 bands of the $3p^2B_1$–$\tilde{X}^2B_1$ transitions of CH_2D and CHD_2have been identified previously at 59940 cm^{-1} and 59920 cm^{-1}, respectively.[47] No signal arising from protiated methyl or either of the heteroisotopic methyl radicals was observed within the detection sensitivity of the experiment. This observation is consistent with the stated isotopic purity of the methyl-d_3-amine (> 99.5% D) and provides evidence that scrambling of the hydrogen atoms does not occur prior to the C–N bond breaking. This contrasts with recent work on acetaldyhyde-d_3 by Heazlewood *et al*., who demonstrated isotopic scrambling and subsequent dissociation on the S_0 surface after initial excitation to S_1 at a range of excitation energies below the T_1 dissociation threshold.[48]

Ab initio stationary points

New *ab initio* calculations have been performed to characterize (at least qualitatively) key features on the S_0, S_1 and T_1 potential energy surfaces of CH_3NH_2. Geometries and harmonic frequencies of minima and transition states on the S_0 and T_1 surfaces were calculated at the (R)CCSD/aug-cc-pVDZ level; equivalent stationary points on the S_1 surface were characterized using the EOM-CCSD method. Energies of stationary points relative to S_0 are shown in Table 2. The S_1 minima and transition state structures, accompanied by the C–N and N–H bond lengths are shown in Figure 5; the equivalent structures on T_1 are almost identical and only the bond lengths are indicated. Including unscaled zero-point energy corrections, the S_1 and T_1 zero-point levels were calculated to be 5.0038 eV and 4.6907 eV above S_0, in excellent agreement with experimental observations of 5.1657 eV and 4.83 eV, respectively.[37,49] The optimized geometries at the S_1 and T_1 minima have the

expected planar configuration of substituents around the nitrogen atom, in contrast to the pyramidal arrangement on S_0. All mimima belong to the C_S point group and have A′ character, with the symmetry plane bisecting the HNH moiety. Barriers to dissociation along the CN and NH bond coordinates were identified on both the S_1 and T_1 surfaces. The CN cleavage transition states maintain the planar configurations around the N atom found at the minima but have extended CN bonds. The CN bond length increases to 1.8149 Å at the transition state on S_1 and to 1.7575 Å on T_1. Other geometrical parameters remain almost constant. On S_1, the transition state lies at a zero-point corrected energy of 5.5853 eV, which means the barrier to direct dissociation of around 0.58 eV calculated at this level of theory is slightly larger than the value of 0.47 eV predicted in the earlier multireference calculations.[19] The analogous transition state on the T_1 surface lies at an energy of 4.9929 eV, slightly below the S_1 zero-point level, and presents a barrier of around 0.30 eV. Along the N–H cleavage pathway, the optimized transition state geometries on both S_1 and T_1 maintain C_S symmetry, but have the ciscoid structure identified by Dunn and Morokuma, the principal difference being the length of the breaking N–H bond. The N–H bond length increases to 1.3748 Å at the transition state on S_1 and to 1.2613 Å on T_1. The barrier to dissociation is calculated to be approximately 0.22 eV on S_1, while the inclusion of harmonic zero-point corrections puts the T_1 transition state 0.04 eV below the T_1 minimum.

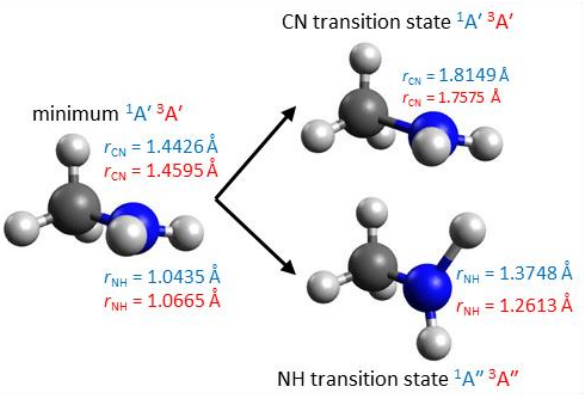

Figure 5. Optimized geometries of the minimum and C–N and N–H cleavage transition states on the S_1 surface. Bond lengths for the S_1 structures and their T_1 equivalents are indicated.

Discussion

Several primary observations can be made on the basis of the experimental data presented: (i) the C–N cleavage pathway is active at all photolysis wavelengths investigated; (ii) CH_3 or CD_3 radicals are formed with vibrational excitation in the high frequency degenerate CH or CD stretch mode, ν_3; (iii) the degree of vibrational excitation in ν_3 is independent of the initially selected vibronic state of the parent amine; and (iv) isotopic scrambling prior to dissociation does not occur.

In the PTS experiments of Waschewsky *et al.*[5], ND_2 fragments arising from dissociation of CH_3ND_2 at a photolysis wavelength of 222 nm were found to have a translational energy distribution that peaked away from zero at ~4 kcal mol^{-1}, indicative of dissociation on a repulsive surface, and cut off at ~17 kcal mol^{-1}, roughly consistent with the energetic threshold that would be expected if electronically excited ND_2* fragments were formed. The mechanism proposed was one of direct dissociation on the upper S_1 surface, avoiding the exit-channel conical intersection that would be expected to funnel population to ground

state products. Based on Dunn and Morokuma's *ab initio* calculations, excitation at 222 nm was thought to provide just enough energy to overcome the C–N barrier on S_1.[19] Prompt (direct) dissociation was also supported by the photofragment angular distribution, which was characterized by an anisotropy parameter of $\beta = -0.4 \pm 0.4$. This value is reduced from the limiting case, but is consistent with a transition dipole moment oriented nearly perpendicular to the C–N bond and some degree of rotation prior to dissociation.

Direct dissociation on the S_1 surface leading to production of CH_3 and electronically excited NH_2* fragments cannot account for the current experimental observations. The observation of vibrationally excited methyl radicals is incompatible with simultaneous production of NH_2* fragments, except at the shortest photodissociation wavelengths used in this work. For example, following initial excitation on the 0_0^0 band at 239.95 nm, the excess energy available for the CH_3 + NH_2 channel is either E_{excess} = 1.468 eV or E^*_{excess} = 0.089 eV, where the asterisk indicates formation of electronically excited aminyl radicals. The equivalent values for excitation of other vibronic bands of methylamine are shown in Table 1. A single quantum of vibrational excitation in ν_3 requires 0.391 eV and only excitation on the $7_0^2 9_0^2$ band, for which E^*_{excess} = 0.498 eV, provides sufficient total energy to produce vibrationally excited CH_3 in conjunction with NH_2 $\tilde{A}^2A_1$. The experimental vibrational distribution, however, extends to three quanta in ν_3 and the majority of CH_3 radical products are vibrationally excited. A similar picture emerges from the CD_3NH_2 photodissociation data. At longer wavelengths, the excess energy available if electronically excited NH_2 $\tilde{A}^2A_1$ is produced is less than the vibrational energy of ν_3 of CD_3 (0.295 eV). Excitation on the 9_0^2 or $7_0^1 9_0^4$ bands can result in CD_3 fragments with at most a single

quantum of vibrational excitation in ν_3, while the observed distribution extends as far as four quanta of ν_3.

The production of nascent CH_3 (CD_3) fragments after excitation to the zero-point and other low-lying levels of S_1 suggests that all *ab initio* calculations significantly over predict the barrier height or that an alternative mechanism leads to the formation of CH_3 (CD_3) + NH_2 products. Based on our *ab initio* calculations, the zero-point corrected barrier of 0.58 eV would prevent direct dissociation at all photolysis energies used in this work. We note that Xiao *et al*. calculate an even higher barrier of 1.00 eV on S_1, although inclusion of zero-point energies would reduce it to some extent.[24] The equivalent barrier on the T_1 surface, however, is calculated to lie lower in energy that the S_1 zero-point level, suggesting that dissociation would be feasible at all excitation wavelengths if intersystem crossing is at least somewhat competitive with predissociation. Within the Condon approximation, assuming only direct spin-orbit coupling, the rate of ISC can be estimated by application of Fermi's golden rule:[50]

$$k_{\mathrm{ISC}} = \frac{2\pi}{\hbar} |M_{\mathrm{SO}}|^2 \rho_{\mathrm{T}_1}(E)$$

Here $M_{\mathrm{SO}} = \langle \mathrm{S}_1 | \hat{H}_{\mathrm{SO}} | \mathrm{T}_1 \rangle$ is the spin-orbit coupling matrix element and $\rho_{\mathrm{T}_1}(E)$ is the vibrational density of states in T_1 at energy E. The Whitten-Rabinovitch approximation[51] (as implemented in the MultiWell-2014 package[52]) with RCCSD/aug-cc-pVDZ harmonic frequencies, is used to evaluate the $\rho_{\mathrm{T}_1}(E)$ for each excitation energy. The value of E is calculated using the *ab initio* singlet-triplet energy difference. The magnitude of M_{SO} was evaluated at geometries that correspond to the S_0, S_1 and T_1 minima as the norm of the 4×4

spin-orbit matrix calculated using the full Breit-Pauli operator and full-valence CASSCF/aug-cc-pVTZ wavefunctions.[53,54] In all geometries, the magnitudes of M_{SO} are small, in agreement with Xiao et al.[24] The calculated values of k_{ISC} are reported in Table 3, where they are compared with predissociation rates derived from previously measured homogeneous line-broadening in 1+1 REMPI spectra of CH_3NH_2.[36] The golden rule calculations suggest energy dependent ISC rates that are ~14,000–400,000 slower than predissociation at the geometry of S_1 (or T_1). We conclude that, although the CN cleavage pathway is minor, the rate of ISC is so slow relative to predissociation that the photodissociation mechanism does not involve ISC to the triplet surface in the Franck-Condon region. We had assumed this previously in our earlier paper identifying the CH_4 + NH $^3\Sigma^-$ channel.[17] We cannot conclusively rule out ISC being important at significantly displaced geometries. Using the larger value for M_{SO} calculated at the pyramidal S_0 geometry leads to faster ISC rates, but they are still ~180–4,700 times slower than predissociation. The difference in magnitude of the spin-orbit coupling matrix elements with geometry suggests that a more detailed treatment that also includes vibronic spin-orbit interaction may yield somewhat faster ISC rates, but it is not obvious that those calculations would likely yield rates competitive with predissociation.

The similarity of the measured methyl vibrational distributions after excitation to different initial vibronic states of S_1 strongly suggests that the same dissociation mechanism is responsible. It also argues against direct passage through the long range exit channel conical intersection (at $r_{CN} \approx 2.5$ Å),[19,24] which might be expected to impart some mode-specificity to the dynamics, as observed in the dominant N–H cleavage pathway.[6,7,10] Dissociative trajectories on S_1 that reach the conical intersection in planar geometries

should lead to CH_3 + NH_2 products directly, in analogy with dissociation of NH_3. In contrast, the adiabatic surfaces remain further apart for trajectories that deviate significantly from planarity, and coupling to S_0 is anticipated to be less favorable, leading to CH_3 + NH_2* products. Suppose, as described by Ahn *et al*.,[10] a potential for the NH_2 wagging mode, ν_9, that is orthogonal to the C–N dissociation coordinate. For relatively low levels of excitation $n\nu_9$, the vibrational wavefunctions for n even will have significant amplitudes at planar geometries, while levels with odd n will have a node at planar geometries and are more likely to sample the conical intersection region in non-planar geometries. Thus, one might expect that the extent of coupling to the lower S_0 adiabat will alternate between being favored or disfavored after initial excitation of modes with even or odd quanta in ν_9. The effect of vibrational excitation in ν_9 on passage through the conical intersection region was also noted by Waschewsky *et al*., who suggested that the anticipated vibrational excitation would lead to trajectories sampling regions of phase space in which the upper and lower adiabats are well separated. However, based on the more recent spectroscopic assignments of Kim and co-workers,[35–37] excitation at 222 nm likely prepares the $2\nu_7+2\nu_9$ mode in S_1, which as an even mode might be expected to favor formation of ground state products. In any event, this point is moot as it seems unlikely that the predicted barrier to direct dissociation on S_1 can be overcome at any of the excitation wavelengths used.

We are forced to conclude therefore, that dissociation occurs on the S_0 surface without the C–N exit channel conical intersection playing a significant role. Unimolecular dissociation of hot ground state molecules would be expected to lead to a statistical partitioning of the excess energy. However, the CH_3 and CD_3 vibrational population distributions derived from the 2+1 REMPI spectra appear not to be statistical; nascent products are formed with

vibrational excitation in the high-frequency mode ν_3 (fundamental wavenumbers of 3161 cm^{-1} and 2381 cm^{-1} for CH_3 and CD_3, respectively), but no measurable population in excited levels of the low-frequency mode ν_2 (606 cm^{-1} and 457 cm^{-1}). A non-statistical dissociation is also consistent with the non-zero peaking translational energy distribution and fragment angular anisotropy measured by Waschewsky et al.[5] The N–H exit-channel conical intersection provides an efficient route to S_0 as discussed by Ashfold and co-workers.[6,7] Dissociative trajectories that begin evolving along the N–H cleavage path will reach the conical intersection region. Those that undergo a nonadiabatic transition to S_0 on the first pass dissociate directly to fast H + CH_3NH fragments. Those that remain on the upper adiabat have insufficient energy to reach the H + CH_3NH^* asymptote (certainly true at the longer wavelengths used in this work) and the dissociation is frustrated. After reaching some extended range of N–H distances, the departing H atom must return to the conical intersection region, whereupon there are additional opportunities to transfer to S_0. Once on S_0, the majority of these returning trajectories will subsequently dissociate to H + CH_3NH, giving rise to the slow fragments that comprise 50-80% of the H-atoms yield.[10] As discussed by Ashfold and co-workers, the sampling of phase space is somewhat curtailed as in the fully statistical limit C–N cleavage would dominate, but this remains a minor pathway.

We suggest that the CH_3 + NH_2 fragments that we and others have observed are a subset of the frustrated N–H cleavage trajectories that undergo a nonadiabatic transition to S_0 on their return after failing to reach the H + CH_3NH^* asymtote. The non-statistical distributions of translational and vibrational energy and angular anisotropy of the CH_3 + NH_2 fragments indicates that energy redistribution on S_0 is incomplete and that

dissociation occurs on a timescale faster than a rotational period. In some sense, this mechanism could be considered as a roaming-type mechanism; initial dissociation along one product pathway is frustrated at long-range prior to the system finding a route to different products. In this case, the route to final products is relatively prompt unimolecular dissociation rather than intramolecular reaction. Currently we lack a good explanation for why the antisymmetric C–H (C–D) stretch in particular is excited in the CH_3 (CD_3) fragment and further experimental and theoretical work is needed to fully explain the detailed partitioning of the available energy.

Conclusions

The state-selective photodissociation dynamics of methylamine (and methyl-d_3-amine) has been investigated using 2+1 REMPI detection of nascent CH_3 (CD_3) products in a time-of-flight mass spectrometer. The spectra show that CH_3 (CD_3) radical products are formed at all photolysis wavelengths and with a significant degree of vibrational excitation in ν_3, the antisymmetric CH (CD) stretch. The degree of vibrational excitation is effectively independent of the mode initially prepared in the excited state of the parent amine and is incompatible with formation of electronically excited NH_2 co-fragments as previously suggested from PTS experiments. In agreement with earlier ab initio calculations, the barrier along the C–N bond on S_1 calculated at the EOM-CCSD/aug-cc-pVDZ level is too large for dissociation to occur directly. The barrier on the triplet surface is lower, but estimated ISC rates are too slow to compete with N–H bond cleavage via a tunneling mechanism, on account of the small spin-orbit coupling constant in the Franck-Condon region. Instead we propose a "semi-direct" photochemical mechanism in which the S_1/S_0

conical intersection along the N–H coordinate provides for rapid population transfer to the ground state. Dissociation to CH_3 and NH_2 can then occur rapidly on S_0, without complete statistical redistribution of the energy. The detailed mechanism that leads to excitation of the antisymmetric C–H stretch, however, remains unclear.

Acknowledgements

The experimental work was performed at the University of Bristol. CM is grateful to Profs. Michael N. R. Ashfold, Andrew. J. Orr-Ewing and David M. Smith, for generously contributing experimental apparatus, and Dr. Fawzi Abou-Chahine for assistance in the laboratory. CM acknowledges the Royal Society for the award of a University Research Fellowship (UF0762608).. JOT thanks EPSRC for providing a Summer Research Bursary.

References

(1) Emeléus, H. J.; Jolley, L. J. 383. The Photochemical Decomposition of Methylamine and Ethylamine. *J. Chem. Soc.* **1935**, 1612–1617.
(2) Wetmore, O. C.; Taylor, H. A. The Photolysis of Methylamine. *J. Chem. Phys.* **1944**, *12*, 61–68.
(3) Johnson, C. I.; Taylor, H. A. The Effect of Temperature on the Photolysis of Methylamine. *J. Chem. Phys.* **1951**, *19*, 613–617.
(4) Michael, J. V.; Noyes, W. A. The Photochemistry of Methylamine. *J. Am. Chem. Soc.* **1963**, *85*, 1228–1233.
(5) Waschewsky, G. C. G.; Kitchen, D. C.; Browning, P. W.; Butler, L. J. Competing Bond Fission and Molecular Elimination Channels in the Photodissociation of CH_3NH_2 at 222 nm. *J. Phys. Chem.* **1995**, *99*, 2635–2645.
(6) Reed, C. L.; Kono, M.; Ashfold, M. N. R. Near-UV Photolysis of Methylamine Studied by H-Atom Photofragment Translational Spectroscopy. *Faraday Trans.* **1996**, *92*, 4897–4904.
(7) Ashfold, M. N. R.; Dixon, R. N.; Kono, M.; Mordaunt, D. H.; Reed, C. L.; Vrakking, M. J. J.; Mills, I. M. Near Ultraviolet Photolysis of Ammonia and Methylamine Studied by H Rydberg Atom Photofragment Translational Spectroscopy [and Discussion]. *Philos. T. Roy. Soc. A* **1997**, *355*, 1659–1676.

(8) Golan, A.; Rosenwaks, S.; Bar, I. Mode-Dependent Enhancement of Photodissociation and Photoionization in a Seven Atom Molecule. *J. Chem. Phys.* **2006**, *125*, 151103–151104.
(9) Golan, A.; Portnov, A.; Rosenwaks, S.; Bar, I. Mode-Dependent Enhancement and Intramolecular Dynamics via Vibrationally Mediated Photodissociation. *Phys. Script.* **2007**, *76*, C79.
(10) Ahn, D.-S.; Lee, J.; Choi, J.-M.; Lee, K.-S.; Baek, S. J.; Lee, K.; Baeck, K.-K.; Kim, S. K. State-Selective Predissociation Dynamics of Methylamines: The Vibronic and H/D Effects on the Conical Intersection Dynamics. *J. Chem. Phys.* **2008**, *128*, 224305–224307.
(11) Marom, R.; Zecharia, U.; Rosenwaks, S.; Bar, I. Vibrational Overtone Spectra of N–H Stretches and Intramolecular Dynamics on the Ground and Electronically Excited States of Methylamine. *J. Chem. Phys.* **2008**, *128*, 154319–10.
(12) Marom, R.; Zecharia, U.; Rosenwaks, S.; Bar, I. Propensity towards H Photofragments in the Photodissociation of CD_3NH_2 Pre-Excited to the First N–H Stretch Overtone. *Mol. Phys.* **2008**, *106*, 213–222.
(13) Marom, R.; Weiss, T.; Rosenwaks, S.; Bar, I. Site-Dependent Photodissociation of Vibrationally Excited CD_3NH_2. *J. Chem. Phys.* **2009**, *130*, 164312–164317.
(14) Marom, R.; Levi, C.; Weiss, T.; Rosenwaks, S.; Zeiri, Y.; Kosloff, R.; Bar, I. Quantum Tunneling of Hydrogen Atom in Dissociation of Photoexcited Methylamine. *J. Phys. Chem. A* **2010**, *114*, 9623–9627.
(15) Marom, R.; Weiss, T.; Rosenwaks, S.; Bar, I. Site-Dependent Photodissociation of Vibronically Excited CD_3NH_2 Molecules. *J. Chem. Phys.* **2010**, *132*, 244310.
(16) Ahn, D.-S.; Lee, J.; Choon Park, Y.; Sup Lee, Y.; Kyu Kim, S. Nuclear Motion Captured by the Slow Electron Velocity Imaging Technique in the Tunnelling Predissociation of the S1 Methylamine. *J. Chem. Phys.* **2012**, *136*, 024306–024306 – 6.
(17) Thomas, J. O.; Lower, K. E.; Murray, C. Observation of NH $X^3\Sigma^-$ as a Primary Product of Methylamine Photodissociation: Evidence of Roaming-Mediated Intersystem Crossing? *J. Phys. Chem. Lett.* **2012**, *3*, 1341–1345.
(18) Kassab, E.; Gleghorn, J. T.; Evleth, E. M. Theoretical Aspects of the Photochemistry of Methanol, Methylamine, and Related Materials. *J. Am. Chem. Soc.* **1983**, *105*, 1746–1753.
(19) Dunn, K. M.; Morokuma, K. Ab Initio Study of the Photochemical Dissociation of Methylamine. *J. Phys. Chem.* **1996**, *100*, 123–129.
(20) Levi, C.; Halasz, G. J.; Vibok, A.; Bar, I.; Zeiri, Y.; Kosloff, R.; Baer, M. An Intraline of Conical Intersections for Methylamine. *J. Chem. Phys.* **2008**, *128*, 244302–244306.
(21) Levi, C.; Halász, G. J.; Vibók, Á.; Bar, I.; Zeiri, Y.; Kosloff, R.; Baer, M. A Novel Intraline of Conical Intersections for Methylamine: A Theoretical Study. *Int. J. Quant. Chem.* **2009**, *109*, 2482–2489.
(22) Levi, C.; Kosloff, R.; Zeiri, Y.; Bar, I. Time-Dependent Quantum Wave-Packet Description of H and D Atom Tunneling in N–H and N–D Photodissociation of Methylamine and Methylamine-d_2. *J. Chem. Phys.* **2009**, *131*, 064302–064307.
(23) Levi, C.; Halász, G. J.; Vibók, A.; Bar, I.; Zeiri, Y.; Kosloff, R.; Baer, M. Intralines of Quasi-Conical Intersections on Torsion Planes: Methylamine as a Case Study. *J. Phys. Chem. A* **2011**, *113*, 6756–6762.
(24) Xiao, H.; Maeda, S.; Morokuma, K. Theoretical Study on the Photodissociation of Methylamine Involving S1, T1, and S0 States. *J. Phys. Chem. A* **2013**, *117*, 5757–5764.

(25) Biesner, J.; Schnieder, L.; Schmeer, J.; Ahlers, G.; Xie, X.; Welge, K. H.; Ashfold, M. N. R.; Dixon, R. N. State Selective Photodissociation Dynamics of Ã State Ammonia. I. *J. Chem. Phys.* **1988**, *88*, 3607–3616.
(26) Biesner, J.; Schnieder, L.; Ahlers, G.; Xie, X.; Welge, K. H.; Ashfold, M. N. R.; Dixon, R. N. State Selective Photodissociation Dynamics of Ã State Ammonia. II. *J. Chem. Phys.* **1989**, *91*, 2901–2911.
(27) Dixon, R. N. Liversidge Lecture. The Dynamics of Photodissociation. *Chem. Soc. Rev.* **1994**, *23*, 375–385.
(28) Mordaunt, D. H.; Ashfold, M. N. R.; Dixon, R. N. Photodissociation Dynamics of Ã State Ammonia Molecules. I. State Dependent Mu-v Correlations in the $NH_2(ND_2)$ Products. *J. Chem. Phys.* **1996**, *104*, 6460–6471.
(29) Mordaunt, D. H.; Dixon, R. N.; Ashfold, M. N. R. Photodissociation Dynamics of Ã State Ammonia Molecules. II. The Isotopic Dependence for Partially and Fully Deuterated Isotopomers. *J. Chem. Phys.* **1996**, *104*, 6472–6481.
(30) Dixon, R. N. Photodissociation Dynamics of Ã State Ammonia Molecules III. A Three-Dimensional Time-Dependent Calculation Using Ab Initio Potential Energy Surfaces. *Mol. Phys.* **1996**, *88*, 949.
(31) Sander, S. P., J. Abbatt, J. R. Barker, J. B. Burkholder, R. R. Friedl, D. M. Golden, R. E. Huie, C. E. Kolb, M. J. Kurylo, G. K. Moortgat, V. L. Orkin and P. H. Wine "Chemical Kinetics and Photochemical Data for Use in Atmospheric Studies, Evaluation No. 17," JPL Publication 10-6, Jet Propulsion Laboratory, Pasadena, 2011 Http://jpldataeval.jpl.nasa.gov.
(32) Tsuboi, M.; Hirakawa, A. Y.; Kawashima, H. The Structure of the Methylamine Molecule in an Excited Electronic State. *J. Mol. Spectrosc.* **1969**, *29*, 216–229.
(33) Hubin-Franskin, M.-J.; Delwiche, J.; Giuliani, A.; Ska, M.-P.; Motte-Tollet, F.; Walker, I. C.; Mason, N. J.; Gingell, J. M.; Jones, N. C. Electronic Excitation and Optical Cross Sections of Methylamine and Ethylamine in the UV–VUV Spectral Region. *J. Chem. Phys.* **2002**, *116*, 9261–9268.
(34) Taylor, D. P.; Bernstein, E. R. On the Low Lying Excited States of Methyl Amine. *J. Chem. Phys.* **1995**, *103*, 10453–10464.
(35) Baek, S. J.; Choi, K.-W.; Choi, Y. S.; Kim, S. K. Vibrational Structures of Predissociating Methylamines (CH_3NH_2 and CH_3ND_2) in Ã States: Free Internal Rotation of CH_3 with Respect to NH_2. *J. Chem. Phys.* **2002**, *117*, 10057–10060.
(36) Baek, S. J.; Choi, K.-W.; Choi, Y. S.; Kim, S. K. Spectroscopy and Dynamics of Methylamine. I. Rotational and Vibrational Structures of CH_3NH_2 and CH_3ND_2 in Ã States. *J. Chem. Phys.* **2003**, *118*, 11026–11039.
(37) Park, M. H.; Choi, K.-W.; Choi, S.; Kim, S. K.; Choi, Y. S. Vibrational Structures of Methylamine Isotopomers in the Predissociative Ã States: CH_3NHD, CD_3NH_2, CD_3NHD, and CD_3ND_2. *J. Chem. Phys.* **2006**, *125*, 084311–084318.
(38) Werner, H.-J.; Knowles, P. J.; Knizia, G.; Manby, F. R.; Schütz, M. Molpro: A General-Purpose Quantum Chemistry Program Package. *Comput. Mol. Sci.* **2012**, *2*, 242–253.
(39) *MOLPRO, Version 2012.1, a Package of Ab Initio Programs, H.-J. Werner, P. J. Knowles, G. Knizia, F. R. Manby, M. Schütz, P. Celani, T. Korona, R. Lindh, A. Mitrushenkov, G. Rauhut, K. R. Shamasundar, T. B. Adler, R. D. Amos, A. Bernhardsson, A. Berning, D. L. Cooper, M. J. O. Deegan, A. J. Dobbyn, F. Eckert, E. Goll, C. Hampel, A. Hesselmann, G. Hetzer, T. Hrenar, G. Jansen, C. Köppl, Y. Liu, A. W. Lloyd, R. A. Mata, A. J. May, S. J. McNicholas, W. Meyer, M.*

E. Mura, A. Nicklass, D. P. O'Neill, P. Palmieri, D. Peng, K. Pflüger, R. Pitzer, M. Reiher, T. Shiozaki, H. Stoll, A. J. Stone, R. Tarroni, T. Thorsteinsson, and M. Wang, , See Http://www.molpro.net.

(40) Hudgens, J. W.; DiGiuseppe, T. G.; Lin, M. C. Two Photon Resonance Enhanced Multiphoton Ionization Spectroscopy and State Assignments of the Methyl Radical. *J. Chem. Phys.* **1983**, *79*, 571–582.

(41) Matsumi, Y.; Obi, K. Relaxation Processes of Electronically Excited Trimethylamine. I. Energy Dependence of Intramolecular Processes in Isolated Molecule. *Chem. Phys.* **1980**, *49*, 87–93.

(42) Clement, S. G.; Ashfold, M. N. R.; Western, C. M.; Johnson III, R. D.; Hudgens, J. W. Triplet Excited States of the NH(ND) Radical Revealed via Two Photon Resonant Multiphoton Ionization Spectroscopy. *J. Chem. Phys.* **1992**, *96*, 5538–5540.

(43) Clement, S. G.; Ashfold, M. N. R.; Western, C. M.; Johnson III, R. D.; Hudgens, J. W. Triplet Rydberg States of the Imidogen Radical Characterized via Two-Photon Resonance-Enhanced Multiphoton Ionization Spectroscopy. *J. Chem. Phys.* **1992**, *97*, 7064–7072.

(44) Fu, H. B.; Hu, Y. J.; Bernstein, E. R. IR/UV Double Resonant Spectroscopy of the Methyl Radical: Determination of ν_3 in the $3p_z$ Rydberg State. *J. Chem. Phys.* **2005**, *123*, 234307–5.

(45) Mebel, A. M.; Lin, S.-H. Excited Electronic States of the Methyl Radical. Ab Initio Molecular Orbital Study of Geometries, Excitation Energies and Vibronic Spectra. *Chem. Phys.* **1997**, *215*, 329–341.

(46) Zhang, W.; Kawamata, H.; Merer, A. J.; Liu, K. IR–UV Double-Resonance of Methyl Radicals and a Determination of the Detection Sensitivity of REMPI Bands. *J. Phys. Chem. A* **2009**, *113*, 13133–13138.

(47) Brum, J. L.; Johnson III, R. D.; Hudgens, J. W. Electronic Spectra of the Heteroisotopic CH_2D and CHD_2 Radicals by Resonance Enhanced Multiphoton Ionization. *J. Chem. Phys.* **1993**, *98*, 3732–3736.

(48) Heazlewood, B. R.; Maccarone, A. T.; Andrews, D. U.; Osborn, D. L.; Harding, L. B.; Klippenstein, S. J.; Jordan, M. J. T.; Kable, S. H. Near-Threshold H/D Exchange in CD_3CHO Photodissociation. *Nat. Chem.* **2011**, *3*, 443–448.

(49) Abuain, T.; Walker, I. C.; Dance, D. F. The Lowest Triplet State in Ammonia and Methylamine Detected by Electron-Impact Excitation. *J. Chem. Soc., Faraday Trans. 2* **1984**, *80*, 641–645.

(50) Marian, C. M. Spin–orbit Coupling and Intersystem Crossing in Molecules. *Comput. Mol. Sci.* **2012**, *2*, 187–203.

(51) Whitten, G. Z.; Rabinovitch, B. S. Accurate and Facile Approximation for Vibrational Energy-Level Sums. *J. Chem. Phys.* **1963**, *38*, 2466–2473.

(52) *MultiWell-2014 Software, 2014, Designed and Maintained by John R. Barker with Contributors Nicholas F. Ortiz, Jack M. Preses, Lawrence L. Lohr, Andrea Maranzana, Philip J. Stimac, T. Lam Nguyen, and T. J. Dhilip Kumar; University of Michigan, Ann Arbor, MI; Http://aoss.engin.umich.edu/multiwell/.*

(53) Zhang, P.; Maeda, S.; Morokuma, K.; Braams, B. J. Photochemical Reactions of the Low-Lying Excited States of Formaldehyde: T_1/S_0 Intersystem Crossings, Characteristics of the S_1 and T_1 Potential Energy Surfaces, and a Global T_1 Potential Energy Surface. *J. Chem. Phys.* **2009**, *130*, 114304–114304 – 10.

(54) Fu, B.; Shepler, B. C.; Bowman, J. M. Three-State Trajectory Surface Hopping Studies of the Photodissociation Dynamics of Formaldehyde on Ab Initio Potential Energy Surfaces. *J. Am. Chem. Soc.* **2011**, *133*, 7957–7968.

Table 1. Vibronic bands used to excite CH_3NH_2 and CD_3NH_2, excess energy available after formation of ground and excited state products and average energy partitioned into CH_3 or CD_3 vibration.

CH_3NH_2					
Band	λ_{phot} / nm	E_{phot} / eV	E_{excess} / eV	E^*_{excess} / eV	$\langle E_{vib} \rangle$ / eV
0_0^0	239.95	5.1671	1.4681	0.0892	0.36±0.07
9_0^1	236.33	5.2463	1.5474	0.1684	0.36±0.06
7_0^1	234.30	5.2917	1.5927	0.2138	0.35±0.07
9_0^2	232.78	5.3262	1.6272	0.2483	0.38±0.07
$7_0^2 9_0^2$	222.38	5.5755	1.8765	0.4975	0.35±0.06
CD_3NH_2					
Band	λ_{phot} / nm	E_{phot} / eV	E_{excess} / eV	E^*_{excess} / eV	$\langle E_{vib} \rangle$ / eV
0_0^0	239.20	5.1833	1.4843	0.1054	0.37±0.05
9_0^1	236.03	5.2528	1.5539	0.1749	0.44±0.05
7_0^1	234.56	5.2859	1.5869	0.2079	0.43±0.05
9_0^2	232.70	5.3281	1.6291	0.2502	0.37±0.05
$7_0^1 9_0^4$	226.59	5.5738	1.8748	0.4959	0.43±0.06

Table 2. *Ab initio* energies calculated at the (EOM-)CCSD/aug-cc-pVDZ level of theory relative to the S_0 minimum. ΔE_{tot} includes unscaled harmonic zero-point corrections.

		Notes	ΔE_{elec} / eV	ΔE_{tot} / eV
CH_3NH_2	S_0	$\tilde{X}^1A'$ pyramidal	0.0000	0.0000
	S_1	$\tilde{A}^1A'$ pyramidal	5.1527	5.0038
	T_1	$\tilde{a}^3A'$ planar	4.9032	4.6907
$CH_3\cdots NH_2$ TS	S_1	$^1A'$ planar	5.8575	5.5853
	T_1	$^3A'$ planar	5.3068	4.9929
$CH_3 + NH_2$		$\tilde{X}^2A_2'' + \tilde{X}^2B_1$	3.6528	3.2321
$CH_3 + NH_2$*		$\tilde{X}^2A_2'' + \tilde{A}^2A_1$	5.0815	4.6761
$CH_3NH\cdots H$ TS	S_1	$^1A''$ ciscoid	5.5740	5.2228
	T_1	$^3A''$ ciscoid	5.0066	4.6506
$H + CH_3NH$		$^2S + \tilde{X}^2A''$	4.4065	3.9956
$H + CH_3NH$*		$^2S + \tilde{A}^2A'$	5.8635	5.4575

Table 3. Spin-orbit coupling matrix elements and estimated ISC rates calculated using Fermi's golden rule. Predissociation rates are derived from homogenous lifetimes reported by Baek et al.[36] Matrix elements were evaluated using calculated using CASSCF/aug-cc-pVTZ wavefunctions at optimized (EOM-)CCSD/aug-cc-pVDZ geometries for S_0, S_1 and T_1.

		M_{SO} @ S_0 / cm^{-1}	M_{SO} @ S_1 / cm^{-1}	M_{SO} @ T_1 / cm^{-1}	
		0.2381	0.0257	0.0272	
Band	$\rho_{T_1}(E)$ / cm	k_{ISC} @ S_0 / 10^9 s^{-1}	k_{ISC} @ S_1 / 10^9 s^{-1}	k_{ISC} @ T_1 / 10^9 s^{-1}	k_{pr} / 10^{12} s^{-1}
0_0^0	0.835	0.560	0.007	0.007	2.63
9_0^1	1.973	1.324	0.015	0.017	2.44
7_0^1	3.147	2.111	0.025	0.027	2.27
9_0^2	4.390	2.945	0.034	0.038	3.03
$7_0^2 9_0^2$	34.387	23.066	0.269	0.300	>4.17

TOC image